Article

Preliminary Performance Analysis of Medium-Range Liquid Hydrogen-Powered Box-Wing Aircraft

Giuseppe Palaia *, **Karim Abu Salem** and **Erasmo Carrera**

Mul2 Group, Department of Mechanical and Aerospace Engineering, Politecnico di Torino, Corso Duca degli Abruzzi 24, 10129 Torino, Italy; karim.abusalem@polito.it (K.A.S.); erasmo.carrera@polito.it (E.C.)
* Correspondence: giuseppe.palaia@polito.it

Abstract: This paper proposes a performance analysis of a medium-range airliner powered by liquid hydrogen (LH_2) propulsion. The focus is on operating performance in terms of achievable payload and range. A non-conventional box-wing architecture was selected to maximize operating performance. An optimization-based multidisciplinary design framework was developed to retrofit a baseline medium-range box-wing aircraft by designing and integrating the fuel tanks needed to store the LH_2; several solutions were investigated for tank arrangement and layout by means of sensitivity analyses. As a main outcome, a performance analysis of the proposed LH_2-powered box-wing aircraft is provided, highlighting the impact of the introduction of this energy carrier (and the integration of the related tank systems) on aircraft operating performance; a comparative study with respect to a competitor LH_2-retrofitted tube-and-wing aircraft is also provided, to highlight the main possible operating differences between the two architectures. The findings reveal that the retrofitted box-wing can achieve long-range flights at the cost of a substantially reduced payload, mainly due to the volume limitations imposed by the installation of LH_2 tanks, or it can preserve payload capacity at the expense of a significant reduction in range, as the trade-off implies a reduction in on-board LH_2 mass. Specifically, the studied box-wing configuration can achieve a range of 7100 km transporting 150 passengers, or shorter ranges of 2300 km transporting 230 passengers. The competitor LH_2-retrofitted tube-and-wing aircraft, operating in the same category and compatible with the same airport apron constraints, could achieve a distance of 1500 km transporting 110 passengers.

Keywords: liquid hydrogen; box wing; aircraft design; optimization; climate neutrality; green aviation; multidisciplinary design; performance analysis

1. Introduction

As a result of the continuously growing concerns about climate change and environmental sustainability, and the constant search for technological advancements, the aviation industry stands at a crossroads. The demand for air travel continues to raise, driven by global connectivity and economic growth [1,2], but so does the imperative to reduce the industry's carbon footprint [3,4]. The pressing need to mitigate the environmental impact of aviation has accelerated the exploration of disruptive non-evolutionary solutions, both in the field of unconventional airframes [5,6] and alternative propulsion technologies [7]. Innovative configurations such as truss-braced wing [8,9], blended wing-body [10,11], and box-wing [12,13] have shown their potential to introduce improvements for aerodynamic and structural performance, and consequently to reduce fuel consumption per passenger transported. Regarding research on innovative propulsion, different technological solutions are currently under deep investigation. Specifically, electrical energy (stored in batteries) and sustainable aviation fuels (SAF) represent a compelling alternative to the current kerosene [14,15]. Electric-powered aircraft, discussed in detail in [16–18], exhibit a main penalizing issue related to the low gravimetric energy density of batteries that introduces large detrimental weight increase; hence, electric or hybrid-electric aircraft may only

be designed to reduce fuel consumption and related emissions for short flight distances, for aircraft belonging to commuter up to the regional category [19–21], whereas some benefit can be gained with much difficulty if medium- and long-range aircraft are considered [22]. However, to assess the actual emissions of hybrid-electric aircraft, the electricity production methods should be taken into account; specifically, a clear transition towards renewably sourced electricity production is compulsory for an actual general reduction in emissions [20,23,24]. Alternative fuels that have the potential to reduce overall aircraft emissions belong to the SAF category. According to Ref. [25], SAF made from organic components (e.g., biomass) can reduce lifecycle emissions by up to 80%, and up to 40% if mixed with current kerosene. Hydrogen is also considered a sustainable fuel, but differently from organic-based fuel, it is typically produced by a process named electrolysis, which extracts hydrogen molecules from water [26]. The main issues related to actual hydrogen utilization are the high cost of the production process and its dependence on electricity, which still relies on a considerable share of fossil sources [27,28]. However, hydrogen, with its high energy density and low emissions, has emerged as a frontrunner in the quest for sustainable aviation [29,30]; this energy carrier, despite its high gravimetric energy density (about three times that of current kerosene [30]), has the main drawback of low volumetric energy density, which makes it difficult to store in an aircraft at room temperature. To limit the volume needed to store hydrogen, two solutions can be adopted: liquid hydrogen and cryo-compressed hydrogen. Both solutions allow for increasing volumetric energy density, but storage is more difficult due to the very low temperature (which is close to absolute zero) and/or high pressure required. Detailed overviews on hydrogen and its applications in aviation are reported in Refs. [31–33]. Encouraged by the potential benefits of the introduction of hydrogen propulsion into civil aircraft, in 1970s, NASA evaluated the impact in terms of payload, range, emissions, cost, and main airport requirements needed to include this technology [34–36]. In 2000, the European project Cryoplane assessed if hydrogen-based aircraft could be a viable solution to mitigate aviation climate impact [37]. Promising results have been achieved in Ref. [38], which found a MTOW reduction of 25–30% with respect a kerosene-based large aircraft (400 pax). In Ref. [39], the design of a long-range hydrogen aircraft is carried out by maintaining the same passenger capacity and range of an Airbus A350 and lengthening the fuselage. In Ref. [40], the design of a short–medium-range hydrogen aircraft, whose fuselage is the same as that of an Airbus A320, is discussed. Ref. [41] presented the assessment of the structural mass of a hydrogen aircraft hosting tanks in the rear part of the fuselage, carrying 250 pax for a range of 1500 nm. Ref. [42] describes a conceptual design framework for different aircraft categories (from regional up to long-range) aimed at designing hydrogen aircraft that host forward and aft tanks. Ref. [43] details a conceptual retrofitting methodology for hydrogen aircraft. As aircraft architectural changes may be needed (or advisable) for the effective installation of cryogenic tanks, in terms of available volumes, external aerodynamic shape, or structural integration, unconventional airframes could be an incisive solution. In Ref. [44], a comprehensive analysis of hydrogen-based blended-wing-body aircraft is presented. In Ref. [45], a conceptual retrofitting methodology for hydrogen-powered box-wing (BW) aircraft is presented: this preliminary study on box-wings lays the foundation for further investigations, which this paper aims at dealing with.

Indeed, one step further in developing efficient low-emission future aircraft can be achieved by integrating advanced propulsion systems with unconventional airframes, as in the case proposed in this research; namely, in this work, the focus is on the box-wing configuration. Box-wing aircraft, also known as PrandtlPlane [12,46] and represented in Figure 1, rely on a lifting system designed according to the best wing system theory proposed by Prandtl [47] and demonstrated by Frediani [48], which identifies the wing system with the minimum induced drag.

Figure 1. Box-wing aircraft artistic representation.

The box-wing architecture was chosen for this study because of the performance capabilities it can offer, based on results available in the literature. Indeed, if such a concept were exploited to achieve an increase in payload, the box-wing would allow for a significant increase in attainable MTOW, while maintaining the same wingspan of conventional competitors and without penalizations in aerodynamic performance [49]; this is due to the higher lifting capability provided by two individual staggered main wings and the related advantages in terms of induced drag reductions. These box-wing features have already been explored for different applications; for the regional aircraft category, coupling the box-wing airframe with a hybrid-electric powertrain, fuel consumption gains are achieved in the whole operating envelope with respect to a tube-and-wing with the same propulsion system, also providing advantages in terms of direct operating cost and CO_2 emissions [50,51]. Regarding the medium-range sector, the results of the PARSIFAL project [52] showed that the box-wing configuration, while maintaining the maximum wingspan compatible with ICAO 'C' airport aprons (i.e., maximum wingspan equal to 36 m), is capable of transporting a payload approximately 66% larger than that of competitors operating in the same sector, providing reductions in fuel consumption per passenger-kilometer estimated at around 22% [49]. The increase in payload is enabled by a re-design of the fuselage, which is not circular but almost elliptical in shape, allowing for considerably more internal volume than in single-aisle aircraft, and also to the increased lifting capability of the box-wing lifting system.

In the present study, it is the possibility of having a larger availability of internal volume, without penalties in terms of overall aircraft size and aerodynamic performance, that may represent the key feature of the box-wing for the integration of LH_2 propulsion [45]. In fact, for LH_2-powered aircraft, the problem of integrating the tanks in the fuselage is crucial, and having a flexible solution in terms of available volume may be decisive for the actual implementation of this technology. This paper aims to provide a performance analysis of the medium-range box-wing hydrogen-powered aircraft by retrofitting the medium-range box-wing aircraft described in [49], hence without modifying its external aerodynamic shape and main structure. An optimization-based design procedure is used to explore the design space and discuss the performance trend of this concept, mainly focusing on the different possibilities of LH_2 tank design and integration; specifically, the performance analysis is configured to provide major focus on the operating capability of such a concept, by discussing the trade-off between available volume for LH_2 tanks, room for passenger seats, and maximum achievable flight range.

The paper is structured as follows: Section 2 describes the state of the art in the design of aeronautical hydrogen technology and the related main challenge, i.e., storage. Section 3 provides an overview of the design methodology; in Section 4, the LH_2 box-wing's performance is discussed, and Section 5 proposes a comparative performance study between box-wing and tube-and-wing hydrogen-based aircraft. Some limitations of the approach here proposed are outlined in Section 6, and finally the conclusions are given in Section 7.

2. H_2 Storage Systems

The design of hydrogen-based aircraft is characterized by the integration of an energy carrier, which has different physical features with respect to current kerosene: in fact,

hydrogen shows a specific energy about three times higher than kerosene, but a lower density, which also depends on the thermodynamic state of the hydrogen, as described in the diagram of Figure 2. Specifically, hydrogen stored at room temperature would be in low density gaseous form and requires a huge volume, which is not compatible with a typical aircraft's available internal volume. To increase its density, hydrogen must be stored as liquid or compressed gas; in both cases, the temperature needed is close to absolute zero (cryogenic condition), and hence hydrogen should be stored in specific tanks capable of maintaining these severe conditions.
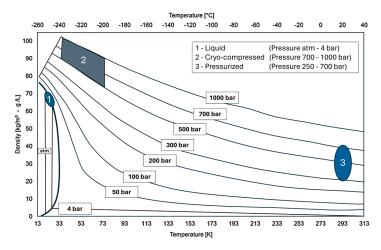

Figure 2. Density-temperature diagram of hydrogen. Image adapted from [53].

Consequently, the cryogenic tank design represents a challenging task, and their onboard integration to transport airplanes increases the complexity of the overall aircraft design. In fact, due to the low available volume, hydrogen cannot be stored in the wing, and hence the most intuitive solution is to provide room for its storage in the fuselage (examples are depicted in Figure 3). This solution, hence, introduces the need to provide a proper design and assessment of the tanks' integration in the fuselage structure; indeed, this solution causes a reduction in the available internal volume for the payload or a redesign of the aircraft's fuselage (with potential penalties in aerodynamic drag), but also an increase in operating empty weight [38,54,55].

Figure 3. Examples of hydrogen tank integration in fuselages: without airframe modifications ((**left**), image adapted from [56]), and with fuselage modification ((**right**), image adapted from [57]).

To store hydrogen in a high-pressurized gaseous state or in liquid state, ad-hoc tanks should be designed. Specifically, for the cryo-compressed gaseous case, tanks should be designed to bear very high internal pressure levels, introducing possible severe structural weight penalties and raising concerns about safety; hence, this solution tends to be discarded for aeronautical applications [31,56]. Internal pressures for cryogenic liquid hydrogen are significantly less critical, but the tank's material should still be robust to embrittlement [58,59]. Embrittlement causes a reduction in material properties (e.g., material yield stress); thus, the reliability of the tanks is a primary goal in safely storing hydrogen. Accordingly, the choice of high strength-to-weight ratio material is relevant for proper tank design; materials such as aluminum alloys, composite materials, stainless steel, and titanium alloys can be ideal candidates to guarantee adequate strength-to-weight ratio

at cryogenic temperature [59]. Liquid hydrogen, selected for the application discussed in this study, allows for increases in volumetric density and can be stored at a pressure close to ambient pressure, as depicted in Figure 2. Nevertheless, the need to maintain temperature to keep the hydrogen in liquid (cryogenic) state requires that the tanks must be properly insulated; indeed, the gradient of temperature between the hydrogen and the external environment generates a heat flow that could cause the LH_2 to boil, i.e., a change in state of the hydrogen from liquid to gaseous. This effect creates a biphasic system composed in the lower part of the tank of liquid hydrogen, and in the upper part of gaseous hydrogen. The boiling effect increases the tank's internal pressure, which must be limited to avoid increased stress in the structural wall of the tank; this is prevented by means of a proper venting valve, which allows for the expulsion of the gaseous hydrogen at a specific preset venting pressure. To reduce the heat flow toward the tank as much as possible, thermal conductivity of the tanks must be as low as possible, so tanks must have a proper shape and ad-hoc insulation material. A shape with a low surface–volume ratio should be considered in order to increase the thermal insulation; regarding the insulation material, the most used are foams [60,61]. Solutions with active refrigeration were investigated in [62], but the increased complexity of the system and the associated increased weight may overcome the potential related benefits. A typical LH_2 tank is composed of (*i*) skin, (*ii*) insulant material, and (*iii*) structural material (see Figure 4). The skin represents a separator between the insulant material and the external volume surrounding the tank, the insulant material aims at increasing the thermal resistivity in order to reduce the heat flow affecting the hydrogen state, and the structural part of the tank aims at bearing the loads (e.g., due to the internal pressure) and should be made of a material that exhibits a high strength-to-weight ratio. Typical materials that can be used for structural walls range from aluminum to composite [31,59]. Currently, there are different ways to insulate the tank: (*i*) closed cell foam, (*ii*) multilayer insulation. Closed cell foams are generally made of polystyrene, polymethacrylimide, or polyurethane, whose thermal conductivity depends on the temperature [57]. Multilayer insulation consists of lightweight reflective sheets assembled in many thin layers. These layers are typically made of polyimide and/or polyester films and allow for a reduction in heat flow [57,58].
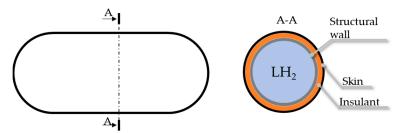

Figure 4. Sketch of the longitudinal section (**left**) and cross-section (**right**) of LH_2 tank.

Two types of tanks can be used to store hydrogen: integral or non-integral tanks. Integral tanks are part of the structural frame of the aircraft and can be used as a load bearing structure; non-integral tanks are vessels attached to the structural frame of the aircraft. There are some differences between them: (*i*) non-integral tanks increase the aircraft's empty weight [42]; (*ii*) non-integral tanks are generally located in the fuselage because the low volume of other areas, such as the wings, does not allow a sufficient amount of hydrogen to be stored, whereas integral tanks can be shaped to be installed in different areas; (*iii*) the mass estimation of an integral tank is not trivial and depends on which area of the aircraft it is integrated, whereas the mass estimation of a non-integral tank is generally independent of its location; (*iv*) the external area of integral tanks is directly wetted by the airflow, whereas non-integral tanks are in contact with the aircraft frame structure, which affects the heat flow [54]. From the above description, it is clear that integral tanks offer a larger design space and would require a deep modification to the aircraft structure. In this study, a retrofitting procedure that does not change the aircraft

structure was considered and, in this respect, non-integral tanks are more suitable. The design and integration of the tanks plays a key role in the development of liquid hydrogen aircraft, as they have a relevant impact on its main performance. In this preliminary study, the investigation of the sizing and integration of the tanks allow for defining some of their main features:

- Weight: by defining the geometry and by means of a thermo-structural sizing approach for pressurized vessels, it is possible to estimate the weight of the tank system, including both structural and insulation contributions.
- Available volumes: the design, the shape, and the number of tanks integrated inside the aircraft enable the computation of the maximum available volume that can be used to store hydrogen.
- Hydrogen thermodynamics: the assessment of the tank's internal hydrogen state dynamics, taking into account both consumption and venting, is helpful to provide indications on the flight endurance achievable using different tank configurations and layouts.
- Payload implications: it is to be expected that the integration of large tanks could result in reductions in the available volume for internal furnishings, and thus in reductions in the number of transported passengers.

Hydrogen, as an energy carrier, can be used in two different ways: as a liquid directly injected in the thermal propulsion system, or as gas that powers fuel cells [31,63], which in turn generate electricity for the electric motors. Both solutions have beneficial effects to reduce aircraft emissions; in fact, during operation, a fuel cell generates only water vapor; liquid hydrogen-based turbomachinery, despite suppressing CO_2 emissions, has the disadvantage of generating NO_x emissions [31,64], whose impact on climate cannot be neglected.

3. Design Methodology for LH_2 Aircraft

3.1. Conceptual Design Framework

In this section, a summary of the design methodology, proposed more in detail in Ref. [45], is given. The developed methodology follows the schematic workflow depicted in Figure 5, and it allows for LH_2 retrofitting of kerosene aircraft (baseline) for both conventional (i.e., tube-and-wing, TW) and any unconventional airframe, such as the box-wing in the present case.
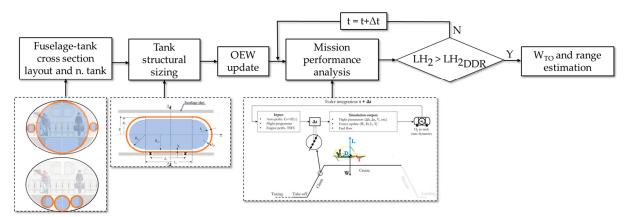

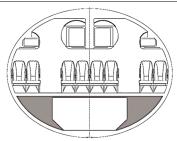**Figure 5.** Scheme of the LH_2 retrofit design workflow.

To initialize the design process, some main assumptions related to the retrofitting strategy adopted in this study have been made; specifically, the following main features of the retrofitted aircraft do not change with respect to the baseline: (*i*) the size of the aircraft, (*ii*) its external shape (tanks are integrated inside the fuselage), (*iii*) the airframe structural mass, and (*iv*) the aerodynamic performance (i.e., aerodynamic polar curves under different operating conditions); furthermore, the LH_2-retrofitted aircraft MTOW should not exceed
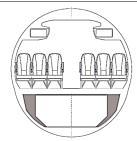
that of the baseline aircraft. For the present study, the reference baseline medium-range BW aircraft is taken from the design study proposed in Ref. [49]; in Table 1, the main features of this BW configuration are reported together with those of a medium-range conventional TW aircraft. The latter is the CeRAS CSR-01 [65], an open access medium-range benchmark aircraft database, and it is used for the comparative assessment presented in Section 5. The fuselage cross-sections reported in Table 1 show the differing shape chosen for the BW, which allows for a larger internal volume for passenger cabin accommodation and/or for the housing of cryogenic hydrogen tanks.

Table 1. Main data of baseline box-wing and tube-and-wing configurations.

Parameter	Box-Wing	Tube-and-Wing
MTOW	125,130 kg$_f$	76,820 kg$_f$
Wingspan	36 m	36 m
Number of pax	308	186
Harmonic range	5720 km	4790 km
Block fuel	21,844 kg	13,670 kg
Fuselage length	44.3 m	37.6 m
Fuselage internal height (max.)	4.05 m	4.05 m
Fuselage internal width (max.)	5.40 m	4.05 m
Aspect ratio (height/width)	0.75	1
Cabin layout	Double aisle, 2-4-2 abreast	Single aisle, 3-3 abreast
Cabin cross-section (*TW is approximated as circular*; *BW is approximated as elliptical*)		

The first step of the retrofitting procedure is the geometry definition and structural sizing of the hydrogen tanks, which are non-integral and are integrated into the fuselage in two different possible modes: "full-section" (FS) layout and "partial-section" (PS) layout. In the FS case, one or more tanks can occupy the entire fuselage cross-section, reducing the space for passengers' cabin and cargo hold, whereas in the PS case, one or more tanks can be hosted in a specific area of the cross-section, e.g., in the cargo hold only without affecting the available volume for passenger seats. Figure 6 depicts a generic schematic example of FS and PS layouts. In addition, one or more groups of tanks (n_t) can be selected by the designer, to be placed in the fore and aft area of the fuselage; an example of two groups of tanks is depicted in Figure 6—center.

The selected general tank geometry is depicted in Figure 7; it consists of a cylindrical part closed by two semi-ellipsoidal endcaps. The cylindrical part, whose length is L_c, is borne by two supports, whose relative distance is d_s, which provide the physical connection between the tanks and fuselage. Figure 7—left shows all the main parameters that define the geometry of the tanks: external radius R, the endcaps aspect ratio f_t (defined according to Equation (1)), the thickness of the insulant material t_{in}, and the thickness of the structural material of cylindrical (t_c) and semi-ellipsoidal (t_e) regions. The tank is modeled as tangential to the internal surface of the fuselage; the tangent point is identified by means of the angle ϕ, the angle that defines the parametric equation of the ellipse, identified as depicted in Figure 7—right; and the radius is defined according to Equation (3).

$$f_t = L_e / R_s \tag{1}$$

$$f = h / w \tag{2}$$

$$R = h\sqrt{f^2 cos^2\phi + sin^2\phi} \tag{3}$$

L_e is the height of the semi-ellipsoidal endcap, R_s is the external radius of the structural material, and f is the height-to-width ratio of the fuselage cross-section.
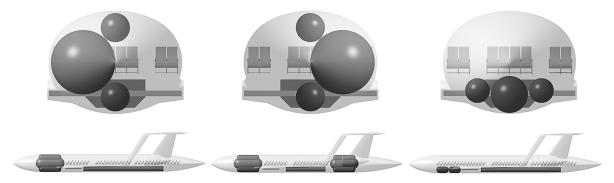

Figure 6. Artistical representations of possible tank–fuselage integration layouts: FS (**left**), FS with two groups of tanks (**center**), PS (**right**).
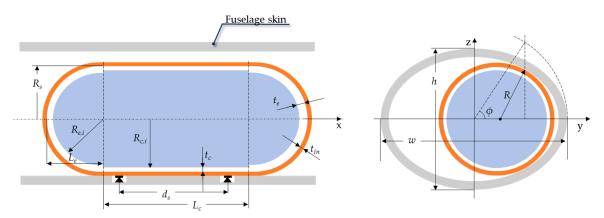

Figure 7. Lateral view (**left**) and cross-section (**right**) of tank integration.

The thickness of the structural material is calculated according to the ASME methodology [66,67], considering the loads defined in [35]. Specifically, the tanks are subject to (*i*) an internal pressure that is higher than the external pressure (at cruising altitude) of a quantity equal to Δp, and (*ii*) inertial loads acting along the vertical direction (*z*-axis of Figure 7) and horizontal direction (*x*-axis of Figure 7) obtained by multiplying the tank weight by a specific load factor (i.e., the ratio between the inertial load and the tank weight). The data related to the loads are reported in Table 2. The structural thickness is sized through an iterative procedure such that the longitudinal and circumferential stresses induced by Δp are not larger than the yield stress material (considering a safe factor of 1.5); then, the maximum tensile stresses induced by the longitudinal and vertical load factors are evaluated and a buckling verification is performed. In case these verifications are not satisfied, the tank thicknesses are updated until convergence is reached. The selected material is the aluminum alloy AA2219, which has yield stress equal to 400 MPa at 20 K; the selected foam material is polystyrene, whose properties are described in [45].

Table 2. Main data used for tank structural design.

Reference Quantity	Value
Tank internal pressure	144.8 kPa [35]
Tank external pressure	22.6 kPa
Vertical load factor	3
Horizontal load factor	6

In the case of FS layout, the presence of the tanks in the fuselage causes a reduction in available volume to accommodate passengers onboard; accordingly, the number of passengers is computed by means of Equation (4), where n_p indicates the number of passengers in the retrofitted aircraft, n_p^* represents the number of passengers in the reference aircraft, k_{n_p} is the number of seats abreast, L_t is the total length of the tanks, n_t is equal to 1 or 2, depending on if there are single or multiple groups of tanks, and l_s is the seat pitch.

$$n_p = n_p^* - k_{n_p} \frac{n_t L_t + l_s}{l_s} \tag{4}$$

$$L_t = L_c + 2L_e \tag{5}$$

By means of Equation (4), operating items' (such as furnishing, seats, galleys, equipment, etc.) weights are recalculated by means of the models proposed in Ref. [68]. The airframe structural weight is kept fixed at that of the baseline, whereas the propulsion system weight is increased by 1%; this derives from the assumption that current turbofans can be modified to run with hydrogen, see Ref. [69], and the increase derives from the necessity to install a dedicated heat exchanger for the hydrogen before its entry to the combustion chamber, as also proposed in [69]. These updates, together with the additional weight introduced by the tanks, allows for recomputing the operating empty weight (OEW) of the retrofitted aircraft. After this stage, as schematically reported in the diagram of Figure 5, the mission simulation of the aircraft is carried out; it includes both the simulation of the longitudinal dynamics of the aircraft and the thermodynamic analysis of the hydrogen in the tanks in each timestep of the mission (more details are reported in the Appendix A). The simulation involves the following assumptions: (*i*) the aircraft is defined as a point mass, i.e., the aircraft model has two degrees of freedom in the vertical plane; (*ii*) specific fuel consumption (SFC) of the engines is considered constant in all phases of the mission and equal to one-third of the baseline aircraft SFC such that the energy spent per unit thrust is equal for kerosene and hydrogen engines [69]; (*iii*) climb and cruise phases are simulated by time-integrating aircraft dynamics equations by means of the Euler method; (*iv*) the thermodynamics of hydrogen are also evaluated concurrently at each timestep of the simulated flight phase (i.e., ground holding, taxi-out, take-off, climb, and cruise), allowing for the assessment of the hydrogen phase, the evaluation of possible boil-off of the liquid hydrogen, the related internal pressure variation, and the computation of the gaseous hydrogen expelled through the venting valve; (*v*) consumption in the descent and diversion phases is considered as a pre-set weight fraction, to avoid iterations of the simulations of the mission, and hence reduce computational time, as detailed in Ref. [45]. Table 3 summarizes the main assumptions on the mission profile. Regarding the hydrogen thermodynamic simulation, the following initial conditions were considered: fill rate of the available volume of the tanks equal to 95%; venting pressure equal to 1.1 of the initial internal pressure (equal to 144.8 kPa [35]).

Table 3. Main data of the mission profile.

Mission Phase	Time Duration	Assumption
Ground holding	28 min	[61]
Taxi-out	15 min	ICAO LTO cycle [70]
Take-off	0.7 min	Full thrust
Climb	Calculated	Pre-set flight program [71]
Cruise	Calculated	$M = 0.79$ @ 11,000 m
Descent	Not simulated	Fixed fraction

The aircraft take-off weight W_{TO} is computed according to Equation (6):

$$W_{TO} = OEW^* + (m_{LH2} + m_p)g \tag{6}$$

where OEW^* is the updated operating empty weight of the retrofitted aircraft, m_{LH2} is the mass of the LH_2 stored onboard, m_p is the payload mass, and g is gravity.

3.2. Optimization-Based Aircraft Retrofitting

This section aims at describing the optimization-based design model, developed in MatLab and built on the design workflow of Section 3.1, used to generally assess the effects of LH_2 tank integration on BW performance. The optimization procedure was set up to size different possible onboard tank layouts, and to assess mission performance for box-wing configurations retrofitted with LH_2 propulsion. Since the external shape of the aircraft is kept the same as the baseline, and therefore the aerodynamic performance and airframe structural weight (excluding tanks) are fixed and known, the optimization procedure defined by Equations (7) and (8) mainly involve design variables related to tank integration, as defined in Table 4; specifically:

$$max \; \mathrm{X}(\boldsymbol{x}) \tag{7}$$

over:

$$l_b \le \boldsymbol{x} \le u_b \tag{8}$$

where X is the flight distance flown in the standard mission, set as objective function to be maximized; the vector of the design variable $\boldsymbol{x}$ is constituted by $\{L_c, f_t, \phi, d_s, t_{in}, R_m\}$; and l_b and u_b are its lower and upper boundaries, respectively. These have been varied within the intervals reported in Table 4 to explore the available design space, to hence design tank layouts with very different features, as discussed in Section 4. Namely, L_c is the length of the cylindrical part of the vessel (as shown in Figure 7—left); f_t is the endcap aspect ratio defined in Equation (1); ϕ is the angular parameter defined in Figure 7—right and allows for defining the tank position within the fuselage cross-section; d_s and t_{in} are the distance between the external supports of the tanks and the thickness of the insulant, respectively, as already defined in Section 3; and R_m is the radius of the smallest tank that can be installed onboard.

L_c and f_t define the longitudinal section geometry of the tanks. By varying the design variables ϕ and R_m, instead, it is possible to change the position, dimension, and number of the tanks in the aircraft cross-section, as depicted in Figure 8; namely, the maximum number of tanks is installed compatibly with the minimum radius R_m. This is a design lever useful for design configurations that need a catwalk between the tanks and the fuselage walls; given the highly innovative nature of hydrogen propulsion technologies for aeronautical applications, current regulations do not establish any recommendations in this regard; however, the room for a catwalk is likely to be ensured [31,72].

Table 4. Upper bound and lower bound of the design variables.

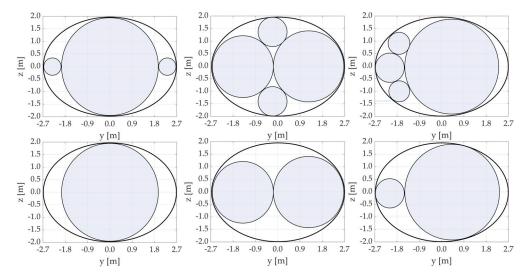| Design Variable	l_b	u_b
L_c [m]	3	15
f_t	0.5	1
ϕ	$-90°$	$90°$
d_s [m]	1.2	5
t_{in} [cm]	3	25
R_m [m]	0.3	1.5

Figure 8. Examples of fuselage tank integration cross-sections; $R_m = 0.09$ m (**top**); $R_m = 0.45$ m (**bottom**).

The optimization framework implemented in MatLab utilizes a local optimization algorithm, specifically, a sequential quadratic programming method, coupled with a multi-start procedure. In this study, the optimization setup is not provided to design a specific optimum solution, but to map the available design space, in order to identify—if any—the major trends between the design parameters related to LH$_2$ tank integration and aircraft mission performance.

In order to assess the performance of the LH$_2$ box-wing, it was decided to evaluate three different possible layouts for tank integration: an FS configuration with a single set of tanks (FS$_1$); an FS configuration with two sets of tanks in the fore and aft areas, respectively (FS$_2$); and a PS configuration, where the tanks are integrated into the aircraft's cargo hold. The first two FS solutions are reasonably the most capable of increasing the aircraft's flight endurance, as they allocate a large internal volume for the storage of liquid hydrogen; however, this could lead to significant payload reductions. For this reason, the PS solution, in which the passenger cabin remains unchanged compared to the baseline, was also investigated; in this case, however, limited flight endurance compared to the baseline could be expected. Even though FS$_2$ could introduce higher penalization in terms of cabin volume reductions, this layout is noteworthy for study as it represents a design lever towards aircraft longitudinal balance.

To verify these assumptions, and to discuss the performance of the aircraft under investigation, the analysis of the results is proposed in Section 4.

4. Results

4.1. Case 1: Full Section Layout

This section describes the main results related to the FS layout configurations with one (fore, labeled FS$_1$) and two sets of tanks (fore and aft, labeled FS$_2$). The main results in

terms of operating performance, i.e., payload and range, are depicted in Figure 9, where each marker represents a retrofitted hydrogen-based box-wing aircraft, designed by means of the optimization tool detailed in Section 3; the red marker indicates the value for the baseline configuration (kerosene-based). Figure 9—left highlights a trade-off correlation between the number of passengers and range; this trade-off depends on two opposite physical properties of hydrogen: high specific energy, i.e., the energy stored for a unit mass, from one side, and low volumetric density from the other. The low volumetric density of hydrogen is the main cause of the necessity of very large tanks when long-range missions are accomplished, as shown in Figure 9—right, which depicts how the range X changes with the tank volume V_t. The necessity to integrate large tanks into the fuselage introduces reductions, even very severe, in the available internal volume for passenger seats; in general, for every tank arrangement, the LH$_2$-retrofitted BW aircraft exhibit a lower payload than the baseline configuration, even for short or very short ranges. These trends on payload and range highlight the main compromise that the introduction of hydrogen as an energy carrier implies for aircraft transportation: LH$_2$ allows for the substitution of current fossil fuel, hence boosting aircraft operations' decarbonization, but the integration of LH$_2$ storage systems implies a sharp reduction in operating performance. In fact, if we analyze the data in Figure 9—left in terms of payload–range pairs, it can be seen that long and very long ranges are achievable with cabin configurations that can accommodate only a few dozen passengers; such solutions are to be discarded because they are of almost no practical interest. A less penalizing trade-off occurs for typical medium-haul routes, e.g., 6000 km (or 4000 km) can be achieved with a passenger count of about 150 (or 190); these figures are close to those typical of aircraft currently operating in the medium-range sector. Shifting to short-haul, the hydrogen-retrofitted box-wing is able to cover a distance of 1500 km with a passenger count of about 230.
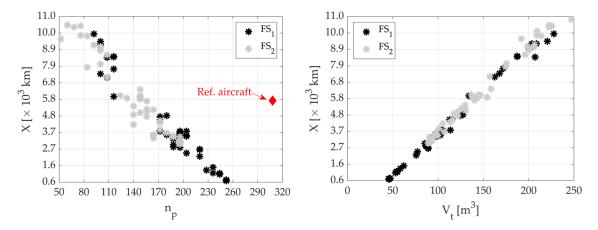

Figure 9. Range vs. number of passengers (**left**) and vs. tanks total volume (**right**).

It is interesting to note that tanks with similar general dimensions can imply different operating performance. In this regard, Figure 10 shows that, for both FS$_1$ and FS$_2$ layouts, there are several tank configurations that have the same total cylindrical length but result in different available volumes for accommodating passenger seats. To discuss this aspect, two couples of configurations, A' and B' for the FS$_1$ group, and C' and D' for the FS$_2$ group, were selected; the tanks belonging to the same FS group exhibit same L_c and R values but different f_t; the latter influences the total length of the tank and hence the available volume for the passenger cabin. The impact of f_t on the internal cabin volume is more relevant for tanks with larger diameter, and its penalizing effect doubles for the FS$_2$ layout. It is therefore the total tank length that has a direct impact on the number of passengers, see Equation (4).
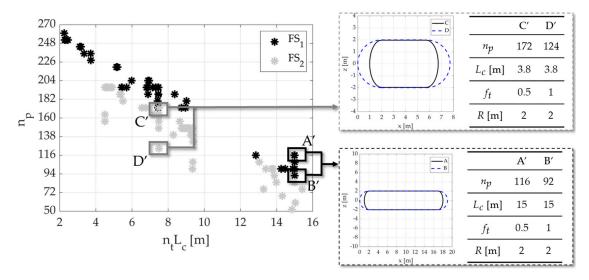
Figure 10. n_p vs. L_c (**left**); detail of the tank shapes for same L_c and R but different f_t (**right**).

A noteworthy aspect of LH$_2$ tank integration is related to the achievable range, with a fixed number of passengers, and hence total tank length; indeed, aircraft integrating tanks having the same total length can have significant differences in maximum range, see Figure 11. This is related to the internal tank volume, which is correlated to the solution the optimizer finds for tank integration in the fuselage cross-section, by acting on ϕ and R_m. Indeed, as presented in Section 3.2, these two parameters define the position and number of tanks (n_{tc}) in the fuselage cross-section, and, consequently, the internal tanks' volume. To underline this aspect, four tank configurations, named A, B, C, and D and shown in Figure 11, are selected; their main features are reported in Table 5. Considering FS$_1$, i.e., cases A and B, the number of tanks in the cross-section n_{tc} is equal to one for both, and the only difference lies in ϕ, which directly affects the radius of the tanks. The differences in terms of tank position and shape introduce a reduction, for the case B, in internal volume and, hence, in energy stored of 22.1% with respect to case A, causing a range reduction of 22.4%. It is interesting to underline that these variables, ϕ and R_m, are very useful for the case a catwalk is required by regulation; consequently, it becomes very easy to add a related constraint to the optimization procedure. Considering the selected example for FS$_2$, i.e., cases C and D, the n_{tc} are different, one and two, respectively; the larger cross-section area in case C allows for storing 23% more energy with an increase of 25.2% in terms of range. In this case, both solutions do not allow for a catwalk.
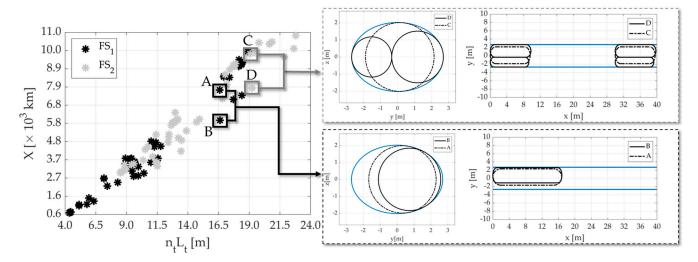

Figure 11. Range vs. total length (**left**); detail of tanks' aircraft arrangement (**right**).

Table 5. Main data of the tanks for cases *A*, *B*, *C*, and *D*.

Parameter	A	B	C	D	
Layout	FS_1	FS_1	FS_2	FS_2	
W_{TO}	92,143 kg$_f$	89,836 kg$_f$	91,816 kg$_f$	89,438 kg$_f$	
X	7730 km	5990 km	9770 km	7810 km	
n_p	116	116	84	84	
L_c	12.85 m	14.98 m	7 m	7.5 m	
t_{in}	9.8 cm	20.9 cm	3.3 cm	10 cm	
f_t	0.99	0.50	0.64	0.75	
ϕ	$-74°$	$-51°$	$83°$	$0°$	
n_{tc}	1	1	1	2	
R	1.98 m	1.84 m	2.02 m	1.52 m	1.18 m
L_t	16.6 m	16.6 m	9.5 m	9.6 m	9.1 m
V_t	172 m^3	134 m^3	107 m^3	56 m^3	31 m^3
Energy stored (E)	1.37×10^6 MJ	1.07×10^6 MJ	1.71×10^6 MJ	1.39×10^6 MJ	

Figure 12—left shows the trends of the mass of vented hydrogen during the evolution of the design mission for the four example cases listed in Table 5. It can easily be seen that the vented mass depends mainly on the thickness of insulation t_{in} with which the tank is coated. Indeed, the thickness of the insulation material affects the thermodynamics of the tank; in particular, the thicker the insulation material, the greater the thermal resistance. Accordingly, the heat flow fraction (i.e., the ratio between the heat flow $\dot{Q}$ and the maximum heat flow $\dot{Q}_{max}$ calculated in the four study cases) towards the liquid hydrogen stored in the tank is reduced in the case of highly thickened insulant foam, as shown in Figure 12—right. High thickened foam reduces the amount of heat received by the liquid hydrogen, so the boiling effect is mitigated, and the amount of mass vented is reduced. Figure 12—right also shows that the heat flow depends on the altitude of the aircraft. On the ground, the temperature of the air surrounding the tank depends on the weather conditions at the airport (in this case study, a standard temperature of 15 °C was considered); the heat flow, which is proportional to the temperature difference between the region inside (i.e., the hydrogen) and outside (i.e., the air) the tank, is maximum in this phase. As altitude increases, the temperature of the air decreases and the temperature difference between the air and the hydrogen becomes progressively smaller; consequently, the heat flow is minimum during the cruise phase. An in-depth discussion of the complex thermodynamic evolution of cryogenic hydrogen inside insulated tanks is described in Refs. [45,60].
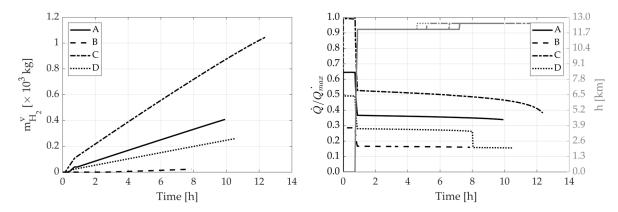

Figure 12. Vented hydrogen mass vs. mission time (**left**) and heat flow fraction vs. time (**right**).

A feature to be discussed regarding LH_2 aircraft is the mass breakdown. Starting from the fuel, LH_2 specific energy is about three times that of the current kerosene; this means that for a unit kg of burned hydrogen, the energy supplied is three times higher than that of kerosene. This is highlighted in Figure 13—left, which reports the range ratio X/X^*, i.e., the ratio between the range accomplished by each LH_2-retrofitted aircraft and the harmonic range of the baseline, see Table 1, vs. the fuel mass ratio m_f/m_f^*, i.e., the ratio between the hydrogen mass burned and vented by each retrofitted BW and the block fuel of the baseline at the design point. The data show that in the case of the range being close to that of the baseline, namely, $X/X^* = 1$, the hydrogen consumption is almost one-third of the fuel consumption of the baseline. The absolute values of hydrogen consumption for the retrofitted aircraft are provided in Figure 13—right.
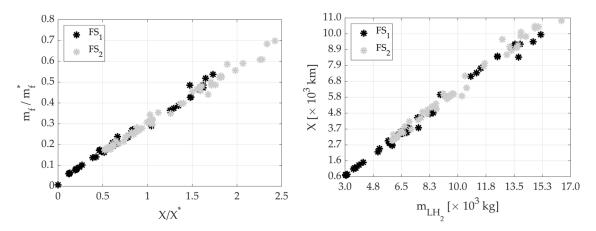

Figure 13. Range ratio vs. fuel mass ratio between retrofitted configurations and reference baseline (**left**) and range vs. mass of loaded hydrogen (**right**).

Figure 14 shows the trends of the mass of tanks (m_t), operating items (m_{op}), and OEW as the range varies. In particular, it can be observed that the mass of the tanks (Figure 14—left) increases as the range raises, as longer tanks are installed to accomplish the mission (cf. Figure 11), whereas the opposite occurs for the mass of the operating items, which tends to decrease (Figure 14—center), as these are directly related to the decreasing passenger number. The increase in the mass of the tanks is larger than the reduction observed for the mass of the operating items; as a result, generally, for all the LH_2-retrofitted BW aircraft, the OEW slightly increases for larger ranges, as shown in Figure 14—right; furthermore, the presence of the tanks introduces OEW increases with respect to the 308-passenger baseline.
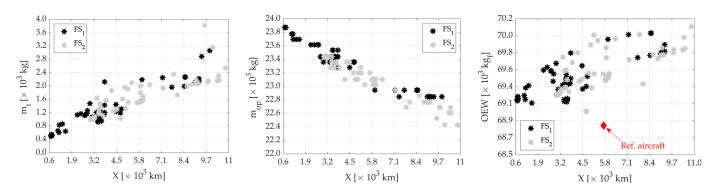

Figure 14. Tank mass (**left**), operating and system mass (**center**), and OEW (**right**) vs. range.

As it is possible to intuitively expect, the fuel mass fraction (Figure 15—left) increases, whereas the payload weight fraction decreases (Figure 15—center), for configurations with longer range. Nevertheless, the already discussed reduction in payload, together with the

significantly lower fuel weight needed due to the three-times higher gravimetric energy density of LH$_2$ than kerosene, lead to a significant reduction in take-off weight compared to the baseline MTOW, see Figure 15—right. These data, therefore, allow for the expectation of further reductions in MTOW if the retrofitting approach is discarded for a complete 'from scratch' redesign of the hydrogen BW aircraft.
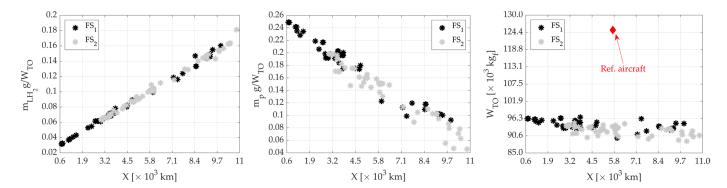

Figure 15. LH$_2$ (**left**) and payload (**center**) weight fractions vs. range; W$_{TO}$ (**right**) vs. range.

An important aspect to evaluate in tank design is the gravimetric efficiency η_t, i.e., the ratio between the mass of fuel stored in the tank and the sum of the mass of the tank and the fuel. Given the same design requirements and constraints for the tanks, having high values of η_t indicates higher storage efficiency. The trend of this parameter as the V_t/t_{in} ratio changes is shown in Figure 16—left, which shows that as the V_t/t_{in} ratio increases (i.e., large tanks and low thickened insulation), tank efficiency increases. The gravimetric efficiency cannot increase significantly because as the internal tank volume increases, the structural mass increases as well, as shown in Figure 16—center. In addition, Figure 16—center shows that insulation mass is generally lower than structural mass, and the discrepancy is much more evident as tank volume increases. The thickness of the insulant affects the effective use of the hydrogen stored onboard, as depicted in Figure 16—right. Indeed, in case of high-thickened foam, the fraction of burned hydrogen η_{H_2} (i.e., the ratio between the burned hydrogen and the sum of burned and vented hydrogen) is almost one, meaning that almost all the stored hydrogen is effectively burned by the engines. In case of low-thickened foam, part of the energy is lost due to the boiling and venting of the hydrogen.
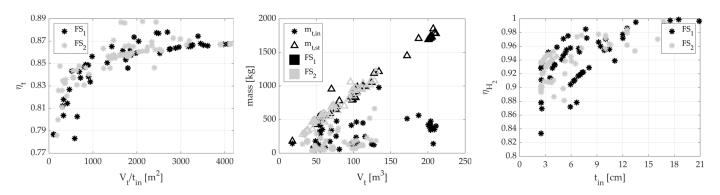

Figure 16. Tank gravimetric efficiency vs. volume-insulant thickness ratio (**left**), mass breakdown of tank vs. tank volume (**center**), and fraction of burned hydrogen vs. insulant thickness (**right**).

An additional element to be discussed is the payload–range energy efficiency (*PREE*), a metric commonly used to assess aircraft productivity [55,73]; *PREE* is defined as the product of flight distance *X* and payload weight per unit of energy spent *E*, see Equation (9).

$$PREE = \frac{m_p g\, X}{E} \tag{9}$$

In the case of LH$_2$ aircraft, to compute the energy spent to fly, we consider both burned and vented hydrogen. The results, depicted in Figure 17—left, show that the retrofitted hydrogen aircraft generally exhibit a significantly lower *PREE* than the reference aircraft; the maximum hydrogen aircraft productivity is located in the range of 2000–5000 km; then, it decreases. The degraded performance of LH$_2$ aircraft with respect to kerosene-based aircraft is mainly related to a lower operating performance in terms of payload–range; Figure 17—center shows that the payload–range product for hydrogen-retrofitted aircraft $n_p X$ divided by the value of the baseline at its design point $n_p^* X^*$ is always significantly lower than 1: this highlights that the payload reduction to allow for tank integration is more impactful than the possible range extensions. Potential reductions in energy spent to fly, achieved for retrofitted aircraft for ranges shorter than 7000 km (see Figure 17—right) do not compensate the degraded operating performance.
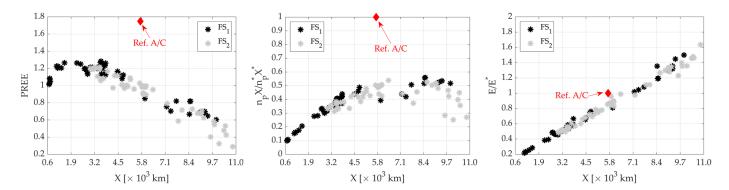

Figure 17. PREE vs. range (**left**) and comparison of PREE's contributions between retrofitted and reference aircraft: payload–range contribution (**center**) and energy contribution (**right**).

In the end, what emerges is that a loss in operating performance is needed if conventional fuel is to be converted to LH$_2$, and thus if it is to cut CO$_2$ emissions. The large disadvantage in terms of volumes required for LH$_2$ storage results in reductions in the payload–range combinations that significantly lower the aircraft's operating envelope. For this specific reason, in this study, it was decided to retrofit a high-capacity aircraft such as the box-wing developed in [49]; in this case, although limitations in operating performance of the retrofitted configurations are apparent, payload–range combinations typical of current short–medium-range (SMR) aircraft can still be achieved. On the other hand, retrofitting current SMR aircraft would result in excessive payload–range reductions, undermining the practical potential of such a retrofit. This aspect will be discussed in Section 5.

4.2. Case 2: Partial Section Layout

This section provides a comparative analysis for the FS (both with one or two groups of tanks) and PS layouts focusing on operating performance and weight. As shown in Figure 18, in the PS layout tanks are located below the cabin floor, in the hold; the constraint imposed by the dimension of the hold implies a strong reduction in tank radius, and, consequently, in the available volume.

Figure 19—left highlights that the configuration retrofitted with the PS layout can fly significantly shorter distances than the FS layout. On the other hand, the PS configuration's tank integration does not reduce passenger cabin volume. The amount of stored hydrogen is much lower in the case of the PS layout (see Figure 19—right), and, consequently, the range is strongly reduced.
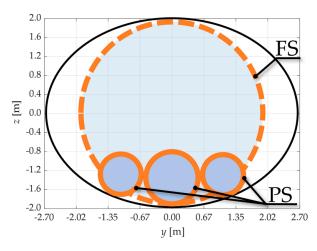
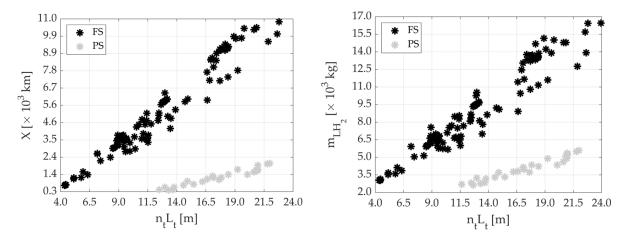**Figure 18.** Generic example of partial section tank integration.

Figure 19. Range (**left**) and mass of LH$_2$ (**right**) vs. tank total length.

The advantage of installing LH$_2$ tanks in the PS layout, hence, lies in the hypothetical non-reduction in the number of passengers, as the tank integration does not affect passenger cabin volume. It has been specified that the non-reduction of the number of passengers is *hypothetical* because the installation of the PS tanks affects the cargo hold's volume, which is necessary to allow for each passenger to travel with at least one piece of baggage. Figure 20—left shows the estimates of the available hold volume V_c and the required hold volume $V_{c,r}$ calculated by considering one unit of luggage per passenger with a volume of 0.113 m^3 [74], for both FS and PS configurations. All the FS configurations comply with the constraint on $V_{c,r}$ due to the fact that the installation of tanks also leads to reductions in the number of passengers. The number of passengers for PS configurations, on the other hand, is constant, and for longer tanks, the available hold volume decreases; for some configurations, therefore, the constraint is not respected, and the layout could be considered unfeasible. The maximum range for feasible PS configurations with 308 passengers is about 930 km, see Figure 20—right. For some configurations for which the constraint is slightly exceeded, some practical solutions could be found, such as a slight reduction in the number of passenger seats to reduce V_c or to allocate some of the cabin volume for baggage loading. In general, however, the volume of the hold is an aspect that cannot be overlooked when dealing with large tank integrations.
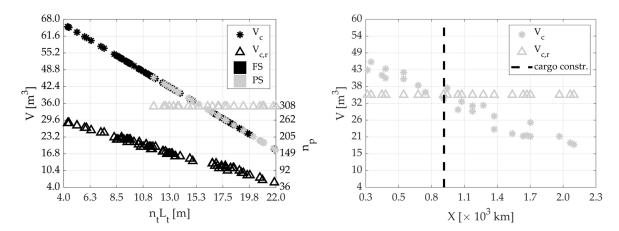
Figure 20. Available vs. required hold volume (**left**) and maximum feasible range for PS (**right**).

In terms of OEW, there are no significant differences between the FS and PS cases (Figure 21—left). This is because the aircraft retrofit only affects the operating items' weight and that of the installed tanks, as depicted in Figure 21—center, whereas the main structural weight of the aircraft remains unchanged. The differences in W_{TO}, see Figure 21—right, are basically related to the differences in mass of hydrogen stored and the number of passengers, and hence in payload weight.
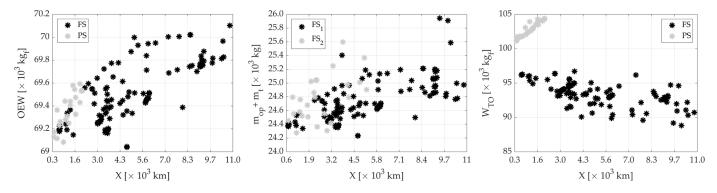

Figure 21. OEW (**left**), operating and tank mass (**center**), and take-off weight (**right**) vs. range.

5. Comparison of Box-Wing and Tube-and-Wing Configuration

In this section, a comparison between hydrogen-powered box-wing and tube-and-wing configurations is presented. The comparative study is carried out by applying both the configurations the methodology describes in Section 3. The main data of the two baseline aircraft are reported in Table 1.

In this case, to provide a general preliminary comparative analysis between the two architectures, sensitivity analysis is used. In this way, rather than having scattered results such as those obtained by means of optimization-driven design (see Section 4), it is possible to select common metrics to discuss the main performance comparison. For both the architectures, a single group of tanks in FS layout is considered, in two different solutions: with and without a catwalk (width equal to 0.80 m). The solutions that maximize cross-section tank area are selected, namely, with $\phi = 90°$ in the case without catwalk for both BW and TW, and $\phi = 80°$ and $\phi = 0°$ in the presence of a catwalk for BW and TW, respectively (see Figure 22).
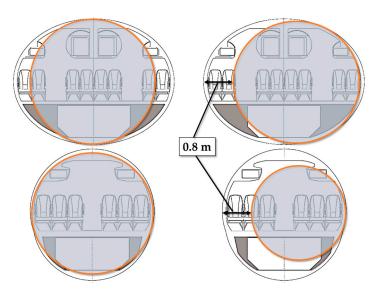
Figure 22. Sketch of no-catwalk (**left**) and catwalk (**right**) solutions for TW an BW.

A sensitivity analysis of two parameters, namely, the ratio between L_c and $2R$ and t_{in}, is carried out, and the related variation range is detailed in Table 6. The first parameter has a direct correlation with the geometry, and the second is the main parameter affecting the hydrogen thermodynamics; both are relevant for tank weight, volume, and hydrogen state evolution. The other parameters are kept fixed, see Table 6.

Table 6. Main parameters for sensitivity analysis.

Parameter	Box-Wing		Tube-and-Wing	
	No catwalk	Catwalk	No catwalk	Catwalk
Catwalk width	0 m	0.8 m	0 m	0.8 m
f_t	0.62	0.62	0.62	0.62
ϕ	90°	80°	90°	0°
d_s/L_c	0.80	0.80	0.80	0.80
$L_c/2R$	1–3	1–3	1–3	1–3
t_{in}	1–25 cm	1–25 cm	1–25 cm	1–25 cm

Figure 23 reports the results of the sensitivity analysis in terms of achieved range for both the BW and TW, with and without catwalk. The results for both the configurations show that the maximum range value reached for any $L_c/2R$ is around t_{in} = 60 mm. Two opposite effects related to the insulant thickness play a key role in this regard: the available internal volume and the vented hydrogen mass during the mission. If t_{in} becomes smaller, the tank internal volume, and hence the stored hydrogen, increases. On the other hand, if the insulant is thinner, the lower thermal resistivity of the tank eases LH$_2$ venting and hence results in greater hydrogen dispersion; the results in terms of vented hydrogen mass are shown in Figure 24. As a secondary effect, big volumes of insulant material can also introduce penalizing weight increases. The specific minimum value found in this case (t_{in} ca. 60 mm) depends on geometrical and material properties; hence, it is not a general reference; on the other hand, this result highlights the need to find a trade-off between thermodynamic efficiency and storage volume for the hydrogen, depending on the specific study case. The effect of $L_c/2R$ on range is quite direct, as R is fixed and increasing L_c allows for larger volumes of stored hydrogen. The differences in range between the TW and BW with the same pairs ($L_c/2R$, t_{in}), in the case without a catwalk (see Figure 23), are mainly related to differences in MTOW, see Table 1; embarking with the same amount

of hydrogen, but having a lower MTOW, allows for the TW configurations to fly longer. The situation is reversed in the case of the presence of the catwalk, see Figure 25, as the radius of the tanks installed on the TW is significantly smaller, leading to tanks with lower volumes than those installed on the corresponding BWs.
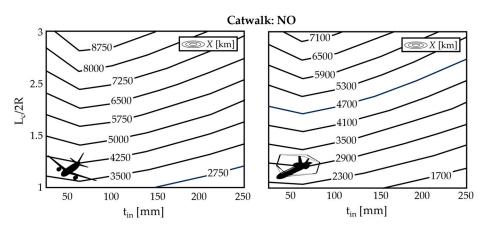
Figure 23. Sensitivity of range to $L_c/2R$ and t_{in} for TW (**left**) and BW (**right**) for *no catwalk* case.
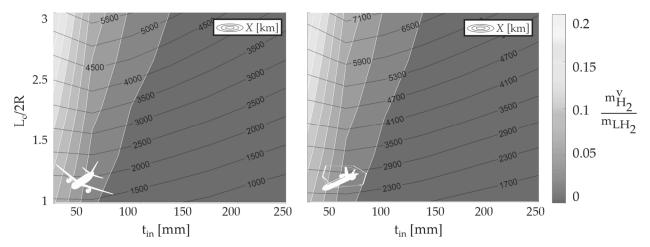
Figure 24. Sensitivity of the vented H_2 to $L_c/2R$ and t_{in} for TW (**left**) and BW (**right**) with catwalk.
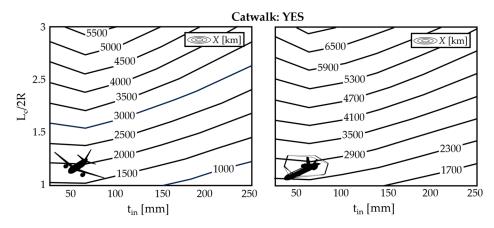
Figure 25. Sensitivity of range to $L_c/2R$ and t_{in} for TW (**left**) and BW (**right**) for *yes catwalk* case.

In every case, however, the TW configuration experiences severe payload reductions, due to the lower availability of internal cabin volume with respect to the BW; Figure 26 shows the contour maps of the number of passengers for TW and BW, together with the range isolines in the case of the presence of a catwalk. TW can embark with a maximum

of 110 passengers for short ranges of about 1500 km (2700 km, without catwalk), reduced to 70 passengers for medium ranges of about 5500 km (8700 km, without catwalk). On the other hand, BW can embark with maximum of 230 passengers for short ranges of about 2300 km, reduced to 150 passengers for medium ranges of about 7100 km. The detailed analysis of the operating potential, hence payload and range pairs, turns out to be of paramount relevance to assess the effective potential to introduce hydrogen-powered aircraft in the medium-range transport sector.
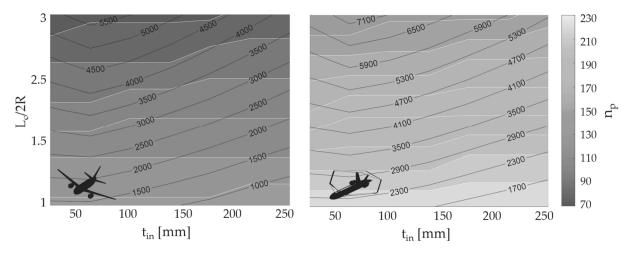

Figure 26. Sensitivity of n_p to $L_c/2R$ and t_{in} for TW (**left**) and BW (**right**) with catwalk.

The results proposed here are consistent with the findings in the literature. Ref. [38] shows that for long-range transport aircraft, a reduction in payload (about 21%) is expected, as well as in harmonic range (about 37%). In Ref. [40], the integration of a fuselage tank in a short-to-medium range aircraft with the same fuselage as the Airbus A320 leads to a reduction in the number of passengers (about 40%) and harmonic range (about 30%) compared to the kerosene version. To counteract the penalty in aircraft operating performance, some authors have lengthened the reference fuselage to accommodate the same number of passengers as the kerosene aircraft. Ref. [39] shows that fuselage–tank integration causes an increase in fuselage length of 37.2% with respect to the baseline aircraft, which negatively affects aircraft OEW (+38.8%) and lift-to-drag ratio (−13.6%). Similar results in terms of increase in OEW were achieved in Ref. [42].

6. Limitations of the Approach

The observations made in Sections 4 and 5 provide interesting insights into the performance potential of liquid hydrogen-powered aircraft. Relevant trade-offs emerge, e.g., between payload and range, and there are macroscopic indications of how and which tanks should be integrated in the fuselage. In general, these indications represent an initial basis for the design's development, and are quite qualitative, given the conceptual nature of the methods and models used. It is clear that, in order to have quantitatively more accurate indications, and to increase the level of detail analyzed, it is necessary to continue with higher-fidelity analysis tools and with the introduction of several aspects that have been neglected in this work. This section aims to briefly summarize and comment on some of these aspects.

First, the actual structural integration between tanks and airframe was neglected. It is indeed necessary to provide the design of reliable attachment systems in the case of non-integral tanks, or to redesign the entire main fuselage structure in the case of integral tanks. In both cases, it is possible to predict non-negligible increases in structural mass, and in general, these aspects cannot be addressed with simplified models and require specific and accurate physical modelling (e.g., FEM models). Furthermore, the safety aspects inherent to both tank–airframe integration and the sizing of the tank itself, with respect to both static

and fatigue loads, must be taken into careful consideration; at present, only assumptions can be made in terms of safety factors, but a design aimed at what will be the certification requirements [59,75] is mandatory. Furthermore, aspects of assembly and installation in the fuselage, inspection, and maintenance cannot be neglected if a feasible concept is to be developed.

The issue of balance and control of the center of gravity for longitudinal and lateral stability and control is of crucial importance in the design of an aircraft; hydrogen-filled tanks are heavy and are intended to be installed in the tip areas of the fuselage, with a significant impact on the position of the center of gravity; in addition, large masses of hydrogen are burnt, with a significant impact on the evolution of the longitudinal position of the center of gravity during the mission. These aeromechanical aspects may affect the actual feasibility of the analyzed solutions and must therefore be taken into account from the earliest design stages, as, for example, proposed in [76] for a box-wing fueled by conventional kerosene.

Finally, it is worth noting that while the detailed study of hydrogen aircraft technological advancement could lead to feasible solutions, it is necessary to interface such developments with the entire infrastructural context surrounding them. In detail, in fact, studies on the capability of airports to receive, store, and handle liquid hydrogen in a safe, efficient, and environmentally friendly manner should be developed concurrently, see Refs. [77,78]. Adaptation of airport facilities to refuel liquid hydrogen aircraft [79] is a crucial aspect and could represent a bottleneck disconnected from aircraft technology development.

7. Conclusions

In this work, the overall operating performance of liquid hydrogen-powered transport aircraft was described. Specifically, by means of a conceptual design workflow developed ad-hoc for such aircraft, the main performance attributes of medium-range box-wing aircraft retrofitted with hydrogen propulsion were described. The choice to use this non-conventional lifting configuration as a reference baseline derives from (*i*) its aerodynamic potential, i.e., the possibility of increasing lift-to-drag ratio and load capacity compared to a conventional aircraft of the same size; (*ii*) the possibility of exploiting these characteristics to design a fuselage with a larger cross-section compared to single-aisle competitors, and thus to have more volume to integrate the bulky hydrogen tanks. The focus, therefore, was given primarily to the design of these tanks and their integration within the aircraft; this aspect, in fact, influences weights, volumes, and hydrogen thermodynamics during the mission, and thus has fundamental implications on performance at the aircraft level.

The results, although conceptual, reveal that if conventional fossil fuel is to be replaced by liquid hydrogen to achieve CO_2 emissions abatement, a trade-off must be paid in terms of reduced operating performance. In particular, a reduction in payload is necessary with respect to the baseline aircraft; if we consider the same harmonic range (5700 km) for the kerosene-fueled box-wing baseline and the hydrogen-fueled one, a 50% reduction in payload can be estimated for the latter; a smaller reduction of about 25% is obtained if, however, a typical flight distance of the short-range category (about 1500 km) is considered. The operating performance penalty is evident. The choice of the box-wing baseline to be retrofitted is justified specifically in this aspect; in fact, although the reduction compared to the reference is significant, this hydrogen-retrofitted configuration still allows for 230 passengers to be transported for 1500 km, or 170 passengers for 4800 km. The latter figure is close to the current scenario for mid-haul aircraft. The same hydrogen retrofitting, carried out on a conventional tube-and-wing aircraft similar to those currently operating in the medium-range category, would result in deteriorating performance figures for an actual entry into service; in fact, for a 4800 km mission, a maximum of 90 passengers could be transported.

It should also be noted that the proposed results are only of conceptual origin; a further increase in detail of the analysis, aimed at introducing aspects and constraints arising from issues related to structural integration, safety, certification, stability, maintenance, and

installation, could further downward revise the operating performance estimates discussed here. On the other hand, the retrofit approach here used could inhibit certain design levers that would instead introduce aspects beneficial to performance. In general, therefore, in the future, such aspects will be modelled and integrated into the design workflow to increase knowledge of the technologies discussed in this paper and provide an enhanced performance estimation scenario to deliver an additional building block in the study of hydrogen-powered aircraft.

List of Symbols and Abbreviations

Symbol	Description	Unit
d_s	Distance between the external supports of the tank	m
E	Energy stored	MJ
f_t	Ratio between L_c and R_s	
g	Standard gravity	
h	Height fuselage cross-section	m
k_{n_p}	Number of abreast seats	
$\boldsymbol{l_b}$	Upper bound vector of design variables	
L_c	Length of the cylindrical part of the tank	m
L_e	Length of the end cap of the tank	m
l_s	Pitch seat	m
L_t	Total length of the tank	m
M	Mach number	
m_{LH_2}	Liquid hydrogen mass stored onboard	kg
m_f	Fuel mass of hydrogen aircraft	kg
m_f^*	Fuel mass of reference aircraft	kg
$m_{H_2}^v$	Vented hydrogen mass	kg
$m_{H_2}^b$	Burned hydrogen mass	kg
m_{op}	Operating mass	kg
m_p	Payload mass	kg
m_t	Tank mass	kg
$m_{t,in}$	Insulant mass of the tank	kg
$m_{t,\text{st}}$	Structural mass of the tank	kg
n_p	Number of passengers	
n_p^*	Number of passengers of reference aircraft	
n_t	Number of groups of tanks	
n_{tc}	Number of tanks in the cross-section	
$\dot{Q}$	Heat flow per unit of time	kW/s
$\dot{Q}_{max}$	Max heat flow per unit of time	kW/s
R	Radius of the tank	m
$R_{c,i}$	Radius of the tank to store hydrogen (cylindrical part)	m
$R_{e,i}$	Radius of the tank to store hydrogen (end cap)	m
R_m	Minimum radius of the tank to install	m
R_s	Radius of the structural part of the tank	m

t_c	Thickness of structural material (cylindrical part)	cm
t_e	Thickness of structural material (end cap)	cm
t_{in}	Insulant thickness	cm
$\boldsymbol{u_b}$	Lower bound vector of design variables	
V_c	Cargo volume	m^3
$V_{c,r}$	Cargo volume requested	m^3
V_t	Tank internal volume	m^3
w	Width fuselage cross-section	m
W_{TO}	Aircraft take-off weight	kg_f
X	Flight distance of hydrogen aircraft	km
X^*	Flight distance of reference aircraft	km
x	Design variables vector	
Δp	Difference between tank internal and external pressure	Pa
η_t	Tank gravimetric efficiency	
η_{H_2}	Fraction of burned hydrogen	
ϕ	Angle that defines the position of the tank	deg

Abbreviation

BW	Box-wing
CeRAS	Central Reference Aircraft System
FS	Full section
ICAO	International Civil Aviation Organization
LH_2	Liquid Hydrogen
LTO	Landing Take-Off
MTOW	Maximum take-off weight
NASA	National Aeronautics and Space Administration
OEW	Operative empty weight
PREE	Payload–range energy efficiency
PS	Partial section
SAF	Sustainable aviation fuel
TW	Tube-and-wing

Appendix A Mission Simulation

The aircraft dynamics equations for the aircraft point-mass model in the longitudinal plane:

$$\begin{cases} \frac{W}{g}\dot{V} = T - D - W\sin\gamma \\ \frac{W}{g}V\dot{\gamma} = L - W\cos\gamma \\ V_x = V\cos\gamma \\ V_z = -V\sin\gamma \\ \dot{W} = -TSFC\,T \end{cases} \tag{A1}$$

where W is the aircraft weight, V the aircraft speed, L is the lift, T the engine thrust, D is the drag, γ is the trajectory slope, g is the gravity acceleration, x and z are the longitudinal and vertical axis, respectively, and *TSFC* is the thrust-specific fuel consumption. The mission parameters, such as the trajectory and performance (e.g., distance covered, fuel consumption, travel time, etc.) are calculated by time, integrating differential equations (A1); a detailed focus on the mission simulation and performance analysis is provided in Ref. [80]. The Euler forward method is used for the numerical integration of the equations of motion; a general formulation of this model is proposed in Equation (A2):

$$y(t+\Delta t) = y(t) + \dot{y}(t)\Delta t \tag{A2}$$

where y is a generic function of time t and $\dot{y}$ represents its time derivative; the mission is discretized in timesteps Δt. The mission is divided in taxi-out, take-off, climb, cruise, descent, approach, landing, and taxi-in, see Figure A1; the flight dynamic equations need a proper set of initial conditions and a flight program selected for each phase, see Table 3; more details are provided in Ref. [49]. The hydrogen thermodynamic model is discussed in

the previous authors' reference [45], in which an appendix is also introduced to provide the related mathematical model.
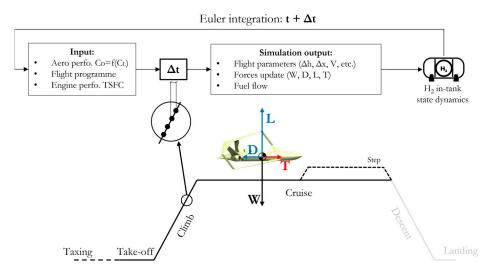

Figure A1. Scheme of the mission simulation; image taken from [45].

A sketch of the flowchart representing the methodology implemented in MATLAB is represented in Figure A2. The whole methodological framework developed is widely discussed in ref. [45].
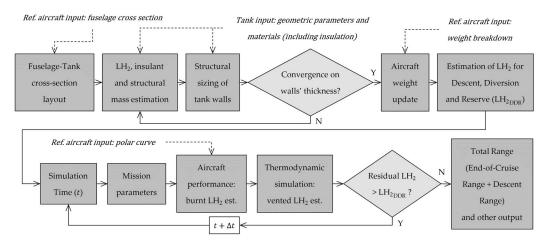

Figure A2. General workflow representing the developed methodology; image adapted from [45].

References

1. IATA. 20 Year Passenger Forecast. Available online: https://www.iata.org/en/publications/store/20-year-passenger-forecast/ (accessed on 21 November 2023).
2. Gössling, S.; Humpe, A.; Fichert, F.; Creutzig, F. COVID-19 and pathways to low-carbon air transport until 2050. *Environ. Res. Lett.* **2021**, *16*, 034063. [CrossRef]
3. Platzer, M.F. A perspective on the urgency for green aviation. *Prog. Aerosp. Sci.* **2023**, *141*, 100932. [CrossRef]
4. Arnaldo, V.; Rosa, M.; Burmaoglu, S.; Tucci, V.; Braga da Costa, C.; Luiz, M.; Gomez, C.; Víctor, F. Flight Path 2050 and ACARE Goals for Maintaining and Extending Industrial Leadership in Aviation: A Map of the Aviation Technology Space. *Sustainability* **2019**, *11*, 2065. [CrossRef]
5. Bravo-Mosquera, P.; Catalano, F.; Zingg, D.W. Unconventional aircraft for civil aviation: A review of concepts and design methodologies. *Prog. Aerosp. Sci.* **2022**, *131*, 100813. [CrossRef]
6. Cavallaro, R.; Demasi, L. Challenges, Ideas, and Innovations of Joined-Wing Configurations: A Concept from the Past, an Opportunity for the Future. *Prog. Aerosp. Sci.* **2016**, *87*, 1–93. [CrossRef]
7. Abu Salem, K.; Palaia, G.; Bravo-Mosquera, P.D.; Quarta, A.A. A Review of Novel and Non-Conventional Propulsion Integrations for Next-Generation Aircraft. *Designs* **2024**, *8*, 20. [CrossRef]

8.   Li, L.; Junqiang, B.; Feng, Q. Multipoint Aerodynamic Shape Optimization of a Truss-Braced-Wing Aircraft. *J. Aircr.* **2022**, *59*, 1179–1194. [CrossRef]

9.   Gur, O.; Bhatia, M.; Schetz, J.A.; Mason, W.H.; Kapania, R.K.; Mavris, D.N. Design Optimization of a Truss-Braced-Wing Transonic Transport Aircraft. *J. Aircr.* **2010**, *47*, 1907–1917. [CrossRef]

10. Martinez-Val, R.; Cuerno, C.; Perez, E.; Ghigliazza, H.H. Potential Effects of Blended Wing Bodies on the Air Transportation System. *J. Aircr.* **2010**, *47*, 1599–1604. [CrossRef]

11. Okonkwo, P.; Smith, H. Review of evolving trends in blended wing body aircraft design. *Prog. Aerosp. Sci.* **2016**, *82*, 1–23. [CrossRef]

12. Frediani, A.; Cipolla, V.; Rizzo, E. The PrandtlPlane Configuration: Overview on Possible Applications to Civil Aviation. In *Variational Analysis and Aerospace Engineering: Mathematical Challenges for Aerospace Design*; Springer Optimization and Its Applications; Buttazzo, G., Frediani, A., Eds.; Springer: Boston, MA, USA, 2012; Volume 66. [CrossRef]

13. Andrews, S.A.; Perez, R.E. Comparison of box-wing and conventional aircraft mission performance using multidisciplinary analysis and optimization. *Aerosp. Sci. Technol.* **2018**, *79*, 336–351. [CrossRef]

14. Afonso, F.; Sohst, M.; Diogo, C.M.A.; Rodrigues, S.S.; Ferreira, A.; Ribeiro, I.; Marques, R.; Rego, F.F.C.; Sohouli, A.; Portugal-Pereira, J.; et al. Strategies towards a more sustainable aviation: A systematic review. *Prog. Aerosp. Sci.* **2023**, *137*, 100878. [CrossRef]

15. Undavalli, V.; Olatunde, O.B.G.; Boylu, R.; Wei, C.; Haeker, J.; Hamilton, J.; Khandelwal, B. Recent advancements in sustainable aviation fuels. *Prog. Aerosp. Sci.* **2023**, *136*, 100876. [CrossRef]

16. Abu Salem, K.; Palaia, G.; Quarta, A.A. Review of hybrid-electric aircraft technologies and designs: Critical analysis and novel solutions. *Prog. Aerosp. Sci.* **2023**, *141*, 100924. [CrossRef]

17. Brelje, B.; Martins, J. Electric, hybrid, and turboelectric fixed-wing aircraft: A review of concepts, models, and design approaches. *Prog. Aerosp. Sci.* **2018**, *104*, 1–19. [CrossRef]

18. Sahoo, S.; Zhao, X.; Kyprianidis, K. A Review of Concepts, Benefits, and Challenges for Future Electrical Propulsion-Based Aircraft. *Aerospace* **2020**, *7*, 44. [CrossRef]

19. Palaia, G.; Abu Salem, K.; Quarta, A.A. Parametric Analysis for Hybrid–Electric Regional Aircraft Conceptual Design and Development. *Appl. Sci.* **2023**, *13*, 11113. [CrossRef]

20. Hoelzen, J.; Liu, Y.; Bensmann, B.; Winnefeld, C.; Elham, A.; Friedrichs, J.; Hanke-Rauschenbach, R. Conceptual Design of Operation Strategies for Hybrid Electric Aircraft. *Energies* **2018**, *11*, 217. [CrossRef]

21. Zaporozhets, O.; Isaienko, V.; Synylo, K. Trends on current and forecasted aircraft hybrid electric architectures and their impact on environment. *Energy* **2020**, *211*, 118814. [CrossRef]

22. Abu Salem, K.; Palaia, G.; Quarta, A.A.; Chiarelli, M.R. Medium-Range Aircraft Conceptual Design from a Local Air Quality and Climate Change Viewpoint. *Energies* **2023**, *16*, 4013. [CrossRef]

23. Gnadt, A.R.; Speth, R.L.; Sabnis, J.S.; Barrett, S.R. Technical and environmental assessment of all-electric 180-passenger commercial aircraft. *Prog. Aerosp. Sci.* **2018**, *105*, 1–30. [CrossRef]

24. Abu Salem, K.; Palaia, G.; Quarta, A.A. Impact of Figures of Merit Selection on Hybrid–Electric Regional Aircraft Design and Performance Analysis. *Energies* **2023**, *16*, 7881. [CrossRef]

25. Overton, J. An Introduction to Sustainable Aviation Fuels, Environmental and Energy Study Institute. Available online: https://www.eesi.org/articles/view/an-introduction-to-sustainable-aviation-fuels (accessed on 14 March 2024).

26. Holladay, J.D.; Hu, J.; King, D.L.; Wang, Y. An overview of hydrogen production technologies. *Catal. Today* **2009**, *139*, 244–260. [CrossRef]

27. Rasul, M.G.; Hazrat, M.A.; Sattar, M.A.; Jahirul, M.I.; Shearer, M.J. The future of hydrogen: Challenges on production, storage and applications. *Energy Convers. Manag.* **2022**, *272*, 116326. [CrossRef]

28. Armaroli, N.; Balzani, V. The hydrogen issue. *ChemSusChem* **2011**, *4*, 21–36. [CrossRef] [PubMed]

29. Bicer, Y.; Dincer, I. Life cycle evaluation of hydrogen and other potential fuels for aircrafts. *Int. J. Hydrogen Energy* **2017**, *42*, 10722–10738. [CrossRef]

30. Nojoumi, H.; Dincer, I.; Naterer, G.F. Greenhouse gas emissions assessment of hydrogen and kerosene-fueled aircraft propulsion. *Int. J. Hydrogen Energy* **2009**, *34*, 1363–1369. [CrossRef]

31. Adler, E.J.; Martins, J.R.R.A. Hydrogen-powered aircraft: Fundamental concepts, key technologies, and environmental impacts. *Prog. Aerosp. Sci.* **2023**, *141*, 100922. [CrossRef]

32. Khandelwal, B.; Karakurt, A.; Sekaran, P.R.; Sethi, V.; Singh, R. Hydrogen powered aircraft: The future of air transport. *Prog. Aerosp. Sci.* **2023**, *60*, 45–59. [CrossRef]

33. Hoelzen, J.; Silberhorn, D.; Zill, T.; Bensmann, B.; Hanke-Rauschenbach, R. Hydrogen-powered aviation and its reliance on green hydrogen infrastructure–Review and research gaps. *Prog. Aerosp. Sci.* **2022**, *47*, 3108–3130. [CrossRef]

34. Berry, W. *A Fuel Conservation Study for Transport Aircraft Utilizing Advanced Technology and Hydrogen Fuel*; NASA-CR-112204; NASA: Hampton, VA, USA, 1972. Available online: https://ntrs.nasa.gov/citations/19730002292 (accessed on 14 March 2024).

35. Brewer, G.D. *Study of the Application of Hydrogen Fuel to Long Range Subsonic Transport Aircraft*; NASA-CR-132559; NASA: Burbank, CA, USA, 1975; Volume 2. Available online: https://ntrs.nasa.gov/citations/19750022090 (accessed on 14 March 2024).

36. Brewer, G.D. *LH2 Airport Requirements Study*; NASA CR-2700; NASA: Burbank, CA, USA, 1976. Available online: https://ntrs.nasa.gov/citations/19770003090 (accessed on 14 March 2024).

37. Klug, H.G.; Faass, R. CRYOPLANE: Hydrogen fuelled aircraft—Status and challenges. *Air Space Eur.* **2001**, *3*, 252–254. [CrossRef]
38. Verstraete, D. Long range transport aircraft using hydrogen fuel. *Int. J. Hydrogen Energy* **2013**, *38*, 14824–14831. [CrossRef]
39. Jagtap, S.S.; Childs, P.R.N.; Stettler, M.E.J. Performance sensitivity of subsonic liquid hydrogen long-range tube-wing aircraft to technology developments. *Int. J. Hydrogen Energy* **2024**, *50*, 820–833. [CrossRef]
40. Barton, D.I.; Hall, C.A.; Oldfield, M.K. Design of a Hydrogen Aircraft for Zero Persistent Contrails. *Aerospace* **2023**, *10*, 688. [CrossRef]
41. Hecken, T.; Balack, P.; Petsch, M.; Zerbst, D. Conceptual loads assessment of aircraft with fuselage integrated liquid hydrogen tank. In Proceedings of the Deutscher Luft-und Raumfahrtkongress 2022, Dresden, Germany, 27–29 September 2022.
42. Onorato, G.; Proesmans, P.; Hoogreef, M.F.M. Assessment of hydrogen transport aircraft. *CEAS Aeronaut. J.* **2022**, *13*, 813–845. [CrossRef] [PubMed]
43. Prewitz, M.; Schwärzer, J.; Bardenhagen, A. Potential analysis of hydrogen storage systems in aircraft design. *Int. J. Hydrogen Energy* **2023**, *48*, 25538–25548. [CrossRef]
44. Karpuk, S.; Ma, Y.; Elham, A. Design Investigation of Potential Long-Range Hydrogen Combustion Blended Wing Body Aircraft with Future Technologies. *Aerospace* **2023**, *10*, 566. [CrossRef]
45. Cipolla, V.; Zanetti, D.; Abu Salem, K.; Binante, V.; Palaia, G. A Parametric Approach for Conceptual Integration and Performance Studies of Liquid Hydrogen Short–Medium Range Aircraft. *Appl. Sci.* **2022**, *12*, 6857. [CrossRef]
46. Frediani, A. The Prandtl Wing, VKI, Lecture Series: Innovative Configurations and Advanced Concepts for Future Civil Transport Aircraft. 2005. Available online: https://perma.cc/XU6F-8YLG (accessed on 14 March 2024).
47. Prandtl, L. *Induced Drag of Multiplanes*; NACA TN 182; NASA: Hampton, VA, USA, 1924.
48. Frediani, A.; Montanari, G. Best wing system: An exact solution of the Prandtl's problem. In *Variational Analysis and Aerospace Engineering*; Springer Optimization and Its Applications; Springer: New York, NY, USA, 2009; Volume 33. [CrossRef]
49. Abu Salem, K.; Cipolla, V.; Palaia, G.; Binante, V.; Zanetti, D. A Physics-Based Multidisciplinary Approach for the Preliminary Design and Performance Analysis of a Medium Range Aircraft with Box-Wing Architecture. *Aerospace* **2021**, *8*, 292. [CrossRef]
50. Palaia, G.; Abu Salem, K.; Quarta, A.A. Comparative Analysis of Hybrid-Electric Regional Aircraft with Tube-and-Wing and Box-Wing Airframes: A Performance Study. *Appl. Sci.* **2023**, *13*, 7894. [CrossRef]
51. Abu Salem, K.; Palaia, G.; Quarta, A.A. Introducing the Box-Wing Airframe for Hybrid-Electric Regional Aircraft: A Preliminary Impact Assessment. *Appl. Sci.* **2023**, *13*, 10506. [CrossRef]
52. Abu Salem, K.; Binante, V.; Cipolla, V.; Maganzi, M. PARSIFAL Project: A Breakthrough Innovation in Air Transport. *Aerotec. Missili Spaz.* **2018**, *97*, 40–46. [CrossRef]
53. Dresden, I.; Kuhn, M. Hydrogen Density Chart. Available online: https://www.ilkdresden.de/leistungen/forschung-und-entwicklung/projekt/wasserstoff-und-methan-versuchsfeld-am-ilk (accessed on 14 March 2024).
54. Silberhorn, D.; Atanasov, G.; Walther, J.N.; Zill, T. Assessment of Hydrogen Fuel Tank Integration at Aircraft Level. In Proceedings of the Deutscher Luft-und Raumfahrtkongress 2019, Darmstadt, Germany, 30 September–2 October 2019.
55. Verstraete, D. On the energy efficiency of hydrogen-fuelled transport aircraft. *Int. J. Hydrogen Energy* **2015**, *40*, 7388–7394. [CrossRef]
56. Airbus. How to Store Liquid Hydrogen for Zero-Emission Flight. Available online: https://www.airbus.com/en/newsroom/news/2021-12-how-to-store-liquid-hydrogen-for-zero-emission-flight (accessed on 14 March 2024).
57. Verstraete, D.; Hendrick, P.; Pilidis, P.; Ramsden, K. Hydrogen fuel tanks for subsonic transport aircraft. *Int. J. Hydrogen Energy* **2010**, *35*, 11085–11098. [CrossRef]
58. Mital, S.K.; Gyekenyesi, J.Z.; Arnold, S.M.; Sullivan, R.M.; Manderscheid, J.M.; Murthy, P.L.N. *Review of Current State of the Art and Key Design Issues with Potential Solutions for Liquid Hydrogen Cryogenic Storage Tank Structures for Aircraft Applications*; NASA Technical Reports Server ID:20060056194; NASA: Hanover, MD, USA, 2006. Available online: https://ntrs.nasa.gov/citations/20060056194 (accessed on 14 March 2024).
59. Tiwari, S.; Pekris, M.J.; Doherty, J.J. A review of liquid hydrogen aircraft and propulsion technologies. *Int. J. Hydrogen Energy* **2024**, *57*, 1174–1196. [CrossRef]
60. Verstraete, D. The Potential of Liquid Hydrogen for Long Range Aircraft Propulsion. Ph.D. Thesis, Cranfield University, Cranfield, UK, 2009. Available online: https://dspace.lib.cranfield.ac.uk/handle/1826/4089 (accessed on 14 March 2024).
61. Winnefeld, C.; Kadyk, T.; Bensmann, B.; Krewer, U.; Hanke-Rauschenbach, R. Modelling and Designing Cryogenic Hydrogen Tanks for Future Aircraft Applications. *Energies* **2018**, *11*, 105. [CrossRef]
62. Millis, M.G.; Tornabene, R.T.; Jurns, J.M.; Guynn, M.D.; Tomsik, T.M.; VanOverbeke, T.J. Hydrogen Fuel System Design Trades for High-Altitude Long-Endurance Remotely-Operated Aircraft. 2009. Available online: https://ntrs.nasa.gov/api/citations/20090013674/downloads/20090013674 (accessed on 14 March 2024).
63. Romeo, G.; Borello, F.; Correa, G.; Cestino, E. ENFICA-FC: Design of transport aircraft powered by fuel cell & flight test of zero emission 2-seater aircraft powered by fuel cells fueled by hydrogen. *Int. J. Hydrogen Energy* **2013**, *38*, 469–479. [CrossRef]
64. Undertaking, H.J. *Fuel Cells and Hydrogen 2 Joint Undertaking, Hydrogen-Powered Aviation–A Fact-Based Study of Hydrogen Technology, Economics, and Climate Impact by 2050*; Publications Office: Luxembourg, 2020. Available online: https://data.europa.eu/doi/10.2843/471510 (accessed on 14 March 2024).
65. Risse, K.; Schäfer, K.; Schültke, F.; Stumpf, E. Central reference aircraft data system (CeRAS) for research community. *CEAS Aeronaut. J.* **2016**, *7*, 121–133. [CrossRef]

66. ASME Boiler and Pressure Vessel Code. *Rules for Construction of Pressure Vessels*; Section VIII, Division 1; American Society of Mechanical Engineers: New York, NY, USA, 2017.

67. ASME Boiler and Pressure Vessel Code. *Rules for Construction of Pressure Vessels (Alternative Rules)*; Section VIII, Division 2; American Society of Mechanical Engineers: New York, NY, USA, 2017.

68. Beltramo, M.; Trapp, D.; Kimoto, B.; Marsh, D. *Parametric Study of Transport Aircraft Systems Cost and Weight*; Report NASA CR151970; NASA: Hampton, VA, USA, 1977. Available online: https://ntrs.nasa.gov/citations/19770019162 (accessed on 14 March 2024).

69. Corchero, G.; Montanes, L. An approach to the use of hydrogen for commercial aircraft engines. *J. Aerosp. Eng.* **2005**, *219*, 35–44. [CrossRef]

70. ICAO. Local Air Quality Technology Standards. 2017. Available online: https://www.icao.int/environmental-protection/Pages/LAQ_TechnologyStandards.aspx (accessed on 14 March 2024).

71. Airbus. *Getting to Grips with Aircraft Performance*; Airbus SAS: Leiden, The Netherlands, 2002. Available online: https://perma.cc/FQ9P-FET4 (accessed on 14 March 2024).

72. Krijnen, J.A.; Astaburuaga, M. Environmental, economical and technical aspects of a cryoplane in the preliminary design phase. In Proceedings of the 23rd ICAS International Congress of Aeronautical Sciences, Toronto, ON, Canada, 8–13 September 2002. Available online: http://www.icas.org/ICAS_ARCHIVE/ICAS2002/PAPERS/7113.PDF (accessed on 14 March 2024).

73. Jagtap, S.; Childs, P.; Stettler, M. Energy performance evaluation of alternative energy vectors for subsonic long-range tube-wing aircraft. *Transp. Res. Part D Transp. Environ.* **2023**, *115*, 103588. [CrossRef]

74. Association of European Airlines. *Short Medium Range Aircraft: AEA Requirements*; Association of European Airlines: Brussels, Belgium, 1989.

75. Spencer, R. Certification considerations for the configuration of a hydrogen-fuelled aeroplane. *Aeronaut. J.* **2023**, *127*, 213–231. [CrossRef]

76. Abu Salem, K.; Palaia, G.; Quarta, A.A.; Chiarelli, M.R. Preliminary Analysis of the Stability and Controllability of a Box-Wing Aircraft Configuration. *Aerospace* **2023**, *10*, 874. [CrossRef]

77. Degirmenci, H.; Uludag, A.; Ekici, S.; Karakoc, T.H. Challenges, prospects and potential future orientation of hydrogen aviation and the airport hydrogen supply network: A state-of-art review. *Prog. Aerosp. Sci.* **2023**, *141*, 100923. [CrossRef]

78. Gu, Y.; Wiedemann, M.; Ryley, T.; Johnson, M.E.; Evans, M.J. Hydrogen-Powered Aircraft at Airports: A Review of the Infrastructure Requirements and Planning Challenges. *Sustainability* **2023**, *15*, 15539. [CrossRef]

79. Hoelzen, J.; Flohr, M.; Silberhorn, D.; Mangold, J.; Bensmann, A.; Hanke-Rauschenbach, R. H2-powered aviation at airports–Design and economics of LH2 refueling systems. *Energy Convers. Manag. X* **2022**, *14*, 100206. [CrossRef]

80. Palaia, G.; Abu Salem, K. Mission Performance Analysis of Hybrid-Electric Regional Aircraft. *Aerospace* **2023**, *10*, 246. [CrossRef]